

# Discrete Boltzmann modelling of compressible reactive flows

Chuangdong Lin<sup>1,2</sup> and Kai H. Luo<sup>2,3</sup>

1. Sino-French Institute of Nuclear Engineering and Technology, Sun Yat-Sen University, Zhuhai 519082, China.
2. Center for Combustion Energy; Key Laboratory for Thermal Science and Power Engineering of Ministry of Education, Department of Energy and Power Engineering, Tsinghua University, Beijing 100084, China.
3. Department of Mechanical Engineering, University College London, Torrington Place, London WC1E 7JE, UK

## 1 Introduction

Reactive flows are ubiquitous in nature, from the forest fires on earth to the supernovae in deep space, and play a key role in human life and society [1]-[3]. Although great achievements have been made in the field, it remains a challenge to study complex reactive flows, especially when compressible, hydrodynamic and thermodynamic coupling effects are under consideration. Traditional hydrodynamic methods suffer from insufficient physical fidelity, while microscopic methods usually incur huge computational costs. One promising class of methods in between is based on the Boltzmann equation, which is a central equation in the kinetic theory [4]-[6].

The Boltzmann equation is a nonlinear integro-differential equation that describes the evolution of particles due to free flight, acceleration, and collisions [4]. It cannot be solved easily due to its complexity, hence a series of simplified physical models have been proposed based on the Boltzmann equation. It is equivalent to a list of infinite moment equations, so that a model has a higher order accuracy if it includes more kinetic moments. They can be roughly divided into two categories: (i) solvers of macroscopic transport equations [4], and (ii) numerical models of the Boltzmann equation [5]-[8].

Discrete Boltzmann method (DBM) is one of the kinetic models, which has been applied to combustion and detonation [9]-[10]. In this work, we develop a novel DBM for compressible reactive flows with various nonequilibrium effects. Compared with previous hybrid schemes where the fluid flow is described by a set of discrete Boltzmann equations and the chemical reaction progress is controlled by another governing equation, this DBM employs one unified set of discrete Boltzmann equations. It has been demonstrated [10]-[12] that the present DBM is physically accurate, computationally efficient, and numerically robust.

## 2 Discrete Boltzmann equation

With the Einstein summation convention, the discrete Boltzmann equation takes the following form.

$$\partial_t f_i^\sigma + v_{i\alpha} \partial_\alpha f_i^\sigma = (\tau^\sigma)^{-1} (f_i^{\sigma eq} - f_i^\sigma) + R_i^\sigma, \quad (1)$$

where the superscript  $\sigma$  indicates the chemical reactant  $A$  and product  $B$ , respectively. The subscript  $t$  denotes time,  $\alpha$  represents the space coordinates  $x$  and  $y$ , respectively.  $\tau^\sigma$  is the relaxation time, and  $\tau^A = \tau^B$  due to momentum conservation.  $f_i^\sigma$  ( $f_i^{\sigma eq}$ ) stands for the discrete (equilibrium) distribution function, with  $i = 1, 2, \dots, 16$ . As shown in Fig. 1, the discrete velocities  $v_i$  read

$$\mathbf{v}_i = \begin{cases} \text{cyc}:(\pm v_a, 0) & i = 1 \sim 4, \\ \text{cyc}:(\pm v_a, \pm v_a) & i = 5 \sim 8, \\ \text{cyc}:(\pm v_b, 0) & i = 9 \sim 12, \\ \text{cyc}:(\pm v_b, \pm v_b) & i = 13 \sim 16, \end{cases} \quad (2)$$

where cyc indicates the cyclic permutation,  $v_a$  and  $v_b$  are tunable parameters to control the values of discrete velocities. In the following text, another parameter should also be introduced, namely,  $\eta_i = 0$ , except  $\eta_i = \eta_a$  for  $i = 5 \sim 8$ .

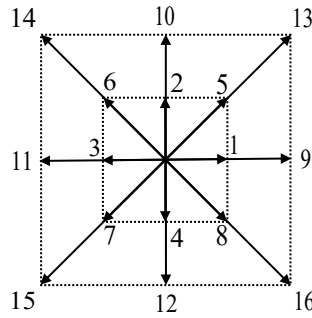


Figure 1. Sketch of the discrete velocities.

For each species  $\sigma$ , the number density is  $n^\sigma = \sum_i f_i^\sigma$ , mass density  $\rho^\sigma = m^\sigma n^\sigma$ , flow velocity  $u_\alpha^\sigma = \sum_i f_i^\sigma v_{i\alpha}^\sigma / n^\sigma$ , and kinetic energy  $E^\sigma = m^\sigma \sum_i f_i^\sigma (v_i^2 + \eta_i^{\sigma 2}) / 2$ . For the mixing, the number density is  $n = \sum_\sigma n^\sigma$ , mass density  $\rho = \sum_\sigma \rho^\sigma$ , flow velocity  $u_\alpha = \sum_\sigma \rho^\sigma u_\alpha^\sigma / \rho$ , and kinetic energy  $E = \sum_\sigma E^\sigma$ . To be consistent with the Navier-Stokes (NS) equations in the hydrodynamic limit, the relations between the discrete equilibrium distribution function  $f_i^{\sigma eq}$  and the equilibrium distribution function  $f^{\sigma eq}$  should be satisfied as below,

$$\sum_i f_i^{\sigma eq} \Psi_i = \iint f^{\sigma eq} \Psi d\mathbf{v} d\eta, \quad (3)$$

with

$$f^{\sigma eq} = \frac{n^{\sigma} m^{\sigma}}{2\pi T} \left( \frac{m^{\sigma}}{2I^{\sigma} \pi T} \right)^{1/2} \exp \left[ -\frac{m^{\sigma} |\mathbf{v} - \mathbf{u}|^2}{2T} - \frac{m^{\sigma} \eta^2}{2I^{\sigma} T} \right] \quad (4)$$

where  $m^{\sigma}$  is the molar mass,  $I^{\sigma}$  counts rovibrational degrees of freedom,  $m^{\sigma} \eta^2 / 2$  corresponds to rovibrational energies. On the left-hand side of Eq. (3) are seven elements  $\Psi_i = 1, \mathbf{v}_i, (\mathbf{v}_i \cdot \mathbf{v}_i + \eta_i^2), \mathbf{v}_i \mathbf{v}_i, (\mathbf{v}_i \cdot \mathbf{v}_i + \eta_i^2) \mathbf{v}_i, \mathbf{v}_i \mathbf{v}_i \mathbf{v}_i, (\mathbf{v}_i \cdot \mathbf{v}_i + \eta_i^2) \mathbf{v}_i \mathbf{v}_i$ , while on the right are  $\Psi = 1, \mathbf{v}, (\mathbf{v} \cdot \mathbf{v} + \eta^2), \mathbf{v} \mathbf{v}, (\mathbf{v} \cdot \mathbf{v} + \eta^2) \mathbf{v}, \mathbf{v} \mathbf{v} \mathbf{v}, (\mathbf{v} \cdot \mathbf{v} + \eta^2) \mathbf{v} \mathbf{v}$ , respectively. Mathematically, Eq. (3) can be rewritten into  $\mathbf{C} \mathbf{f}^{\sigma eq} = \mathbf{M}_{\mathbf{f}}^{\sigma eq}$ , as a consequence,

$$\mathbf{f}^{\sigma eq} = \mathbf{C}^{-1} \mathbf{M}_{\mathbf{f}}^{\sigma eq} \quad (5)$$

with a square matrix  $\mathbf{C}$  that acts as a bridge between  $\mathbf{f}^{\sigma eq} = (f_1^{\sigma eq} \ f_2^{\sigma eq} \ \dots \ f_{16}^{\sigma eq})^T$  and the kinetic moments  $\mathbf{M}_{\mathbf{f}}^{\sigma eq} = (M_{f_1}^{\sigma eq} \ M_{f_2}^{\sigma eq} \ \dots \ M_{f_{16}}^{\sigma eq})^T$ .

Moreover, to calculate the reaction term  $R_i^{\sigma}$ , we employ the following relation,

$$\sum_i R_i^{\sigma} \Psi_i = \iint R^{\sigma} \Psi d\mathbf{v} d\eta, \quad (6)$$

with

$$R^{\sigma} = f^{\sigma eq} \frac{n^{\sigma'}}{n^{\sigma}} + f^{\sigma eq} \frac{-3I^{\sigma} kT + m^{\sigma} I^{\sigma} |\mathbf{v} - \mathbf{u}|^2 + m^{\sigma} \eta^2}{2I^{\sigma} T^2} T', \quad (7)$$

where  $n^{\sigma'}$  and  $T'$  characterize the change rate of number density and temperature due to chemical reactions, respectively. The elements  $\Psi_i$  and  $\Psi$  in Eq. (6) are the same as those in (3). Similarly, Eq. (6) could be rewritten as  $\mathbf{C} \mathbf{R}^{\sigma} = \mathbf{M}_{\mathbf{R}}^{\sigma}$ , hence

$$\mathbf{R}^{\sigma} = \mathbf{C}^{-1} \mathbf{M}_{\mathbf{R}}^{\sigma}, \quad (8)$$

with  $\mathbf{R}^{\sigma eq} = (R_1^{\sigma} \ R_2^{\sigma} \ \dots \ R_{16}^{\sigma})^T$ , and  $\mathbf{M}_{\mathbf{R}}^{\sigma} = (M_{R_1}^{\sigma} \ M_{R_2}^{\sigma} \ \dots \ M_{R_{16}}^{\sigma})^T$ .

For simplicity, the chemical reactant and product are denoted as  $A$  and  $B$ , respectively. To control the chemical reaction, i.e.,  $A \rightarrow B$ , the Arrhenius function is employed

$$\omega = k_{ov} n^A \exp \left( -\frac{E_a}{T} \right) \quad (9)$$

where  $k_{ov}$  represents the reaction coefficient, and  $E_a$  is the effective activation energy. Consequently,

$$n^{\sigma'} = S^{\sigma} \omega \quad (10)$$

$$E' = \sum_{\sigma} \frac{2 + I^{\sigma}}{2} (n^{\sigma} T)' = \omega Q \quad (11)$$

with  $(S^A, S^B) = (-1, 1)$ , and  $Q$  the heat release per unit mass of chemical reactant. Hence,

$$T' = \left[ 2\omega Q - T \sum_{\sigma} (2 + I^{\sigma}) n^{\sigma'} \right] \left[ \sum_{\sigma} (2 + I^{\sigma}) n^{\sigma} \right]^{-1} \quad (12)$$

It is worth noting that, in addition to the recovery of NS equations in the hydrodynamic limit, the DBM has the capability to provide various thermodynamic nonequilibrium information. Specifically,  $\Delta_2^{\sigma} = \sum_i (f_i^{\sigma} - f_i^{\sigma eq}) \mathbf{v}_i^{\sigma} \mathbf{v}_i^{\sigma}$  is related to the viscous stress tensor,  $\Delta_3^{\sigma} = \sum_i (f_i^{\sigma} - f_i^{\sigma eq}) \mathbf{v}_i^{\sigma} \mathbf{v}_i^{\sigma} \mathbf{v}_i^{\sigma}$  the nonorganised heat flux,  $\Delta_{3,1}^{\sigma} = \sum_i (f_i^{\sigma} - f_i^{\sigma eq}) \mathbf{v}_i^{\sigma} \cdot \mathbf{v}_i^{\sigma} \mathbf{v}_i^{\sigma}$  the flux of nonorganised heat flux,  $\Delta_{4,2}^{\sigma} = \sum_i (f_i^{\sigma} - f_i^{\sigma eq}) \mathbf{v}_i^{\sigma} \mathbf{v}_i^{\sigma} \cdot \mathbf{v}_i^{\sigma} \mathbf{v}_i^{\sigma}$  the flux of viscous stress flux.

### 3 Results and Discussions

To demonstrate the capability of the DBM, we perform two tests. The first is a one-dimensional steady detonation, where numerical results are compared with the ZND theory [1]. The second is a two-dimensional explosion, which aims to validate the conservation of mass, momentum, and energy.

#### 3.1 Steady Detonation

Firstly, we simulate a steady detonation wave that travels forward with a Mach number  $Ma = 2.71102$ . In front of the detonation wave,  $0.1 \leq x \leq 1$ , is the chemical reaction with density  $\rho = 1$ , velocity  $\mathbf{u} = 0$ , and temperature  $T = 1$ . The chemical heat release per unit mass of chemical reactant is  $Q = 4$ . Behind the detonation wave,  $0 \leq x < 0.1$ , is the chemical product with physical quantities  $(\rho, u_x, u_y, T) = (1.56244, 1.15470, 0, 3.01066)$ , which are obtained from the Rankine-Hugoniot relations. The resolution is  $N_x \times N_y = 10000 \times 1$ , the spatial step  $\Delta x = \Delta y = 10^{-4}$ , the temporal step  $\Delta t = 5 \times 10^{-6}$ , the relaxation time  $\tau^{\sigma} = 4 \times 10^{-5}$ , the rovibrational degrees of freedom  $I^{\sigma} = 3$ , the reaction coefficient  $k_{ov} = 800$ , the effective activation energy  $E_a = 1$ , and the parameters  $(v_a, v_b, \eta_a) = (1.5, 5.5, 6.0)$ . Furthermore, the inflow and outflow boundary conditions are imposed on the left and right sides, respectively. The period boundary condition is employed in the  $y$  direction.

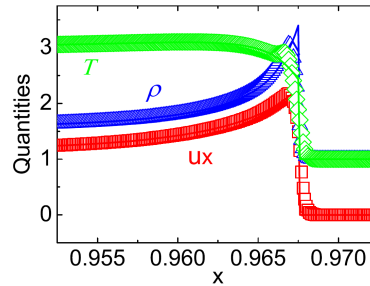


Figure 2. Profiles of the detonation wave.

Figure 2 illustrates the profiles of density (triangles), horizontal velocity (squares), and temperature (diamonds) in the evolution of the detonation at the time constant  $t = 0.275$ . The solid lines denote the ZND solutions [1]. We can find a good agreement between the DBM results and the ZND solutions in the whole

region except the von Neumann peak. The physical reason is that our DBM takes account of viscosity, heat conduction, and various thermodynamic nonequilibrium effects, hence there is a smooth continuity around the detonation wave. In contrast, the ZND theory [1] ignores the viscosity, heat conduction, and various thermodynamic nonequilibrium effects, and assumes there is a sharp discontinuity at the detonation front.

### 3.2 Explosion wave

Next, let us simulate an explosion wave in a square cavity with length and width  $L_x = L_y = 0.08$ . The spatial resolution is  $N_x = N_y = 201$ , the time step  $\Delta t = 2 \times 10^{-5}$ , the relaxation time  $\tau^\sigma = 10^{-4}$ , the rovibrational degrees of freedom  $I^\sigma = 3$ , the reaction coefficient  $k_{ov} = 1.2 \times 10^5$ , the effective activation energy  $E_a = 15$ , and the parameters  $(v_a, v_b, \eta_a) = (0.9, 3.5, 6.0)$ . In addition, the specular reflection boundary condition is chosen for the walls. Theoretically, there is no mass or heat transfer through the walls.

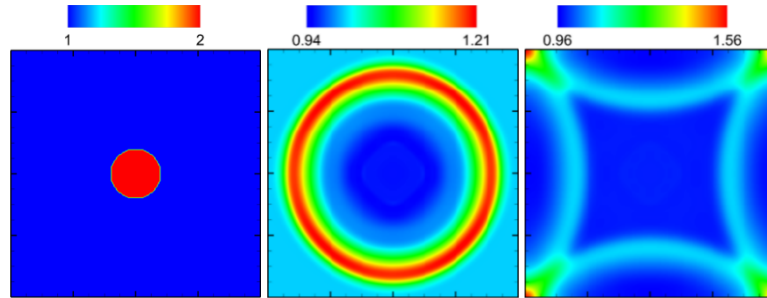


Figure 3. Pressure contours at time constants  $t = 0, 0.02$ , and  $0.04$  in the evolution of explosion.

Initially, the chemical product with  $(\rho, u_x, u_y, T) = (0.5, 0, 0, 4)$  is located in the center of the computational domain with radius  $R < L_x/10$ . Around the circular area is the chemical reactant with  $(\rho, u_x, u_y, T) = (1, 0, 0, 1)$ . The chemical heat release per unit mass of chemical reactant is  $Q = 2$ . Figure 3 displays the pressure,  $p = nT$ , in the evolution of explosion at time constants  $t = 0, 0.02$ , and  $0.04$ , from left to right, respectively. As shown in the middle panel, the explosive wave propagates outward as time goes on. The pressure is high around the explosive wave, and is low inside the explosive wave. The rightmost panel shows that, after the explosive wave collides with walls, it turns into reflected wave and travels inwards. Obviously, the simulated explosive phenomenon is qualitatively right.

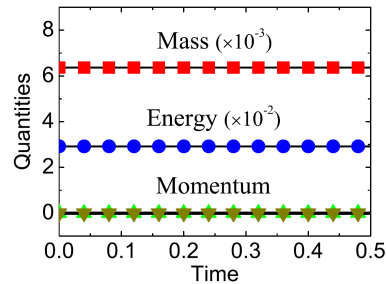


Figure 4. Conservative quantities in the evolution of explosion.

To further have a quantitative verification, Fig. 4 demonstrates the evolution of conservative quantities in the cavity. The squares stands for mass, the circles for energy, the upper and lower triangles for momentum

in  $x$  and  $y$  directions, respectively. The lines represent corresponding theoretical results. It is evident that the numerical and theoretical results coincide with each other. For example, the DBM gives  $(\rho, \rho u_x, \rho u_y, E) = (6.36580, 1.5 \times 10^{-7}, 1.5 \times 10^{-7}, 2.91851)$  at time  $t = 0, 0.2$ , which are quite close to the theoretical results  $(6.36456, 0, 0, 2.91883)$ , respectively.

## 4 Conclusions

An efficient, accurate, and robust DBM is constructed for compressible reactive flows with various hydrodynamic and thermodynamic nonequilibrium effects. In addition to being consistent with the traditional NS equations in the continuity limit condition, the DBM contains various significant thermodynamic nonequilibrium effects beyond the NS equations. It is a kinetic model based on a unified set of discrete Boltzmann equations that describe reactive flows. Two types of benchmarks, that is, one-dimensional steady detonation and two-dimensional explosive, are adopted to demonstrate the capability of this model.

## References

- [1] Law, CK. (2006). *Combustion physics*. Cambridge University Press, Cambridge (ISBN-13 978-0-521-87052-8).
- [2] Yao S, Wang J. (2016). Multiple ignitions and the stability of rotating detonation waves. *Appl. Therm. Eng.* 108: 927.
- [3] Zheng H, Qi L, Zhao N, et al. (2018). A Thermodynamic Analysis of the Pressure Gain of Continuously Rotating Detonation Combustor for Gas Turbine. *Appl. Sci.* 8: 535.
- [4] Struchtrup H. (2005). *Macroscopic transport equations for rarefied gas flows*. Springer, Berlin (ISBN-13 978-3-540-24542-1).
- [5] Lin C, Xu A, Zhang G, et al. (2016). Double-distribution-function discrete Boltzmann model for combustion. *Combust. Flame.* 164: 137.
- [6] Lin C, Luo K. (2018). Mesoscopic simulation of nonequilibrium detonation with discrete Boltzmann method. *Combust. Flame.* 198: 356.
- [7] Yang L, Shu C, Wu J, et al. (2017). Comparative study of discrete velocity method and high-order lattice Boltzmann method for simulation of rarefied flows. *Comput. Fluids.* 146: 125.
- [8] Jaiswal S, Alexeenko A, Hu J. (2019). A discontinuous Galerkin fast spectral method for the full Boltzmann equation with general collision kernels. 378: 178.
- [9] Yan B, Xu A, Zhang G, Ying Y, et al. (2013). Lattice Boltzmann model for combustion and detonation. *Front. Phys.* 8: 94.
- [10] Lin C, Xu A, Zhang G, et al. (2014). Polar coordinate lattice Boltzmann kinetic modeling of detonation phenomena. *Commun. Theor. Phys.* 62: 737.
- [11] C. Lin, K. H. Luo, L. Fei and S. Succi, "A multi-component discrete Boltzmann model for nonequilibrium reactive flows," *Scientific Reports* 7 (1), Article No. 14580 (2017).
- [12] C. Lin and K. H. Luo. (2018). MRT discrete Boltzmann method for compressible exothermic reactive flows. *Computers and Fluids* 166: 176.